Supplement of Atmos. Chem. Phys., 26, 10455–10476, 2026
https://doi.org/10.5194/acp-26-10455-2026-supplement


Atmospheric Chemistry and Physics
Open Access

*Supplement of*

# Applying satellite observations to improve bottom-up national emission inventories for methane: application to Colombia

**Sarah E. Hancock et al.**

*Correspondence to:* Sarah E. Hancock (sarahhancock@g.harvard.edu)

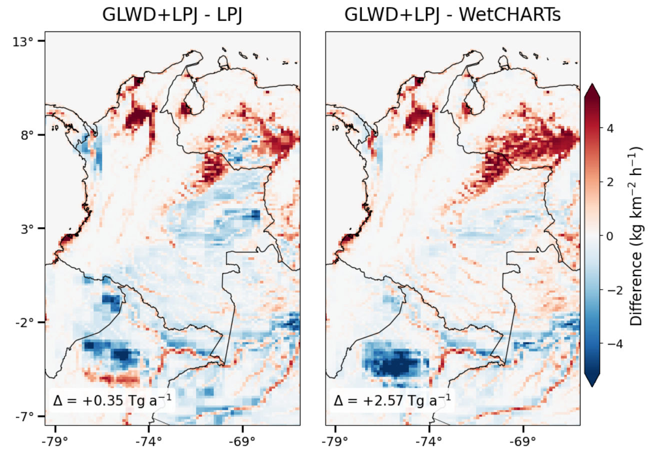


**Figure S1: Differences between the GLWD+LPJ wetland prior emissions and the LPJ and WetCHARTs wetland prior emissions over the full inversion domain. Positive values indicate regions where GLWD+LPJ yields larger prior emissions, and negative values indicate regions where GLWD+LPJ yields smaller prior emissions. Panel annotations report the domain-total emission difference in Tg $a^{-1}$.**

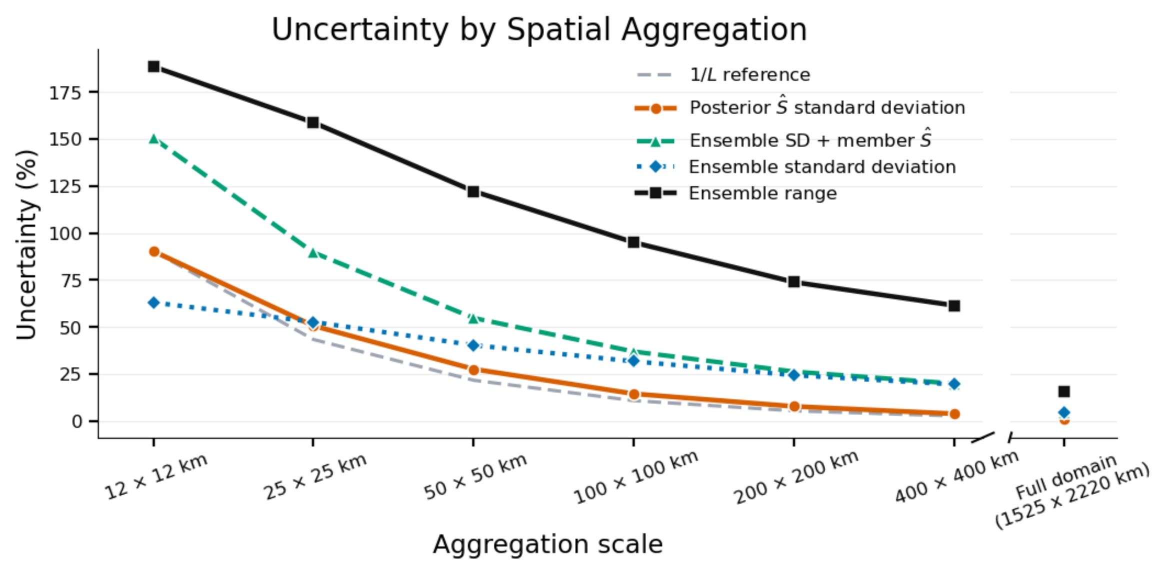


**Figure S2. Dependence of posterior uncertainty on spatial aggregation scale, expressed as percent uncertainty in aggregated mean methane flux. The orange curve shows the posterior error standard deviation derived from the base inversion posterior covariance matrix, $\hat{\mathbf{S}}$. The blue curve shows the standard deviation of aggregated posterior fluxes across the inversion ensemble. The green curve shows the ensemble standard deviation including the posterior variance of each ensemble member. The black curve shows the ensemble range, defined as the difference between the maximum and minimum aggregated posterior fluxes across ensemble members. The gray dashed curve shows a $1/L$ dependence on aggregation scale for reference where $L$ is the characteristic horizontal length scale of the spatial aggregation. We use the ensemble range as the uncertainty estimate for the inversion because it is the most conservative measure.**

**Ensemble standard deviation including member $\hat{\mathbf{S}}$:**

$$\sigma_{\text{ens,tot}} = \sqrt{\mathrm{Var}(\mu_m) + \mathrm{mean}(\sigma_m^2)},$$

**where $\mu_m$ is the aggregated posterior mean for ensemble member $m$ and $\sigma_m^2$ is the corresponding aggregated posterior variance derived from that member's $\hat{\mathbf{S}}$.**

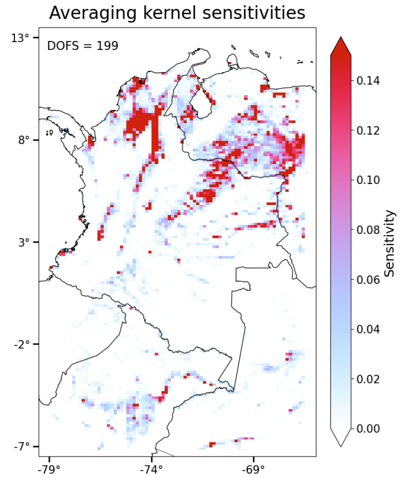


**Figure S3: Averaging kernel sensitivities on the native inversion grid over the full inversion domain. These sensitivities are given by the diagonal elements of the full averaging kernel matrix, *A*, and indicate the extent to which posterior emissions are constrained by the observations rather than the prior estimate. Values closer to 1 indicate stronger observational constraint, while values closer to 0 indicate weaker constraint. This map shows only the diagonal sensitivities and does not depict off-diagonal averaging kernel terms, which represent coupling among grid cells. These off-diagonal terms can be especially important at high resolution, where neighboring state elements are often only partially resolved independently and observational information can spread across multiple nearby grid cells.**

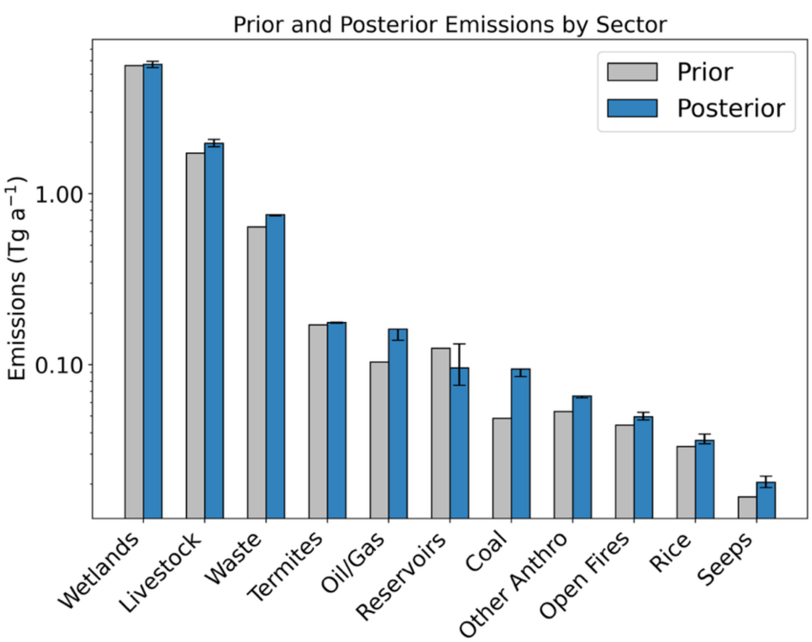


**Figure S4: National methane emissions in Colombia by sector. Prior emissions are from inventories described in Table 1. Posterior emissions are from our base inversion of TROPOMI+GOSAT observations, with error bars representing the uncertainty range.**

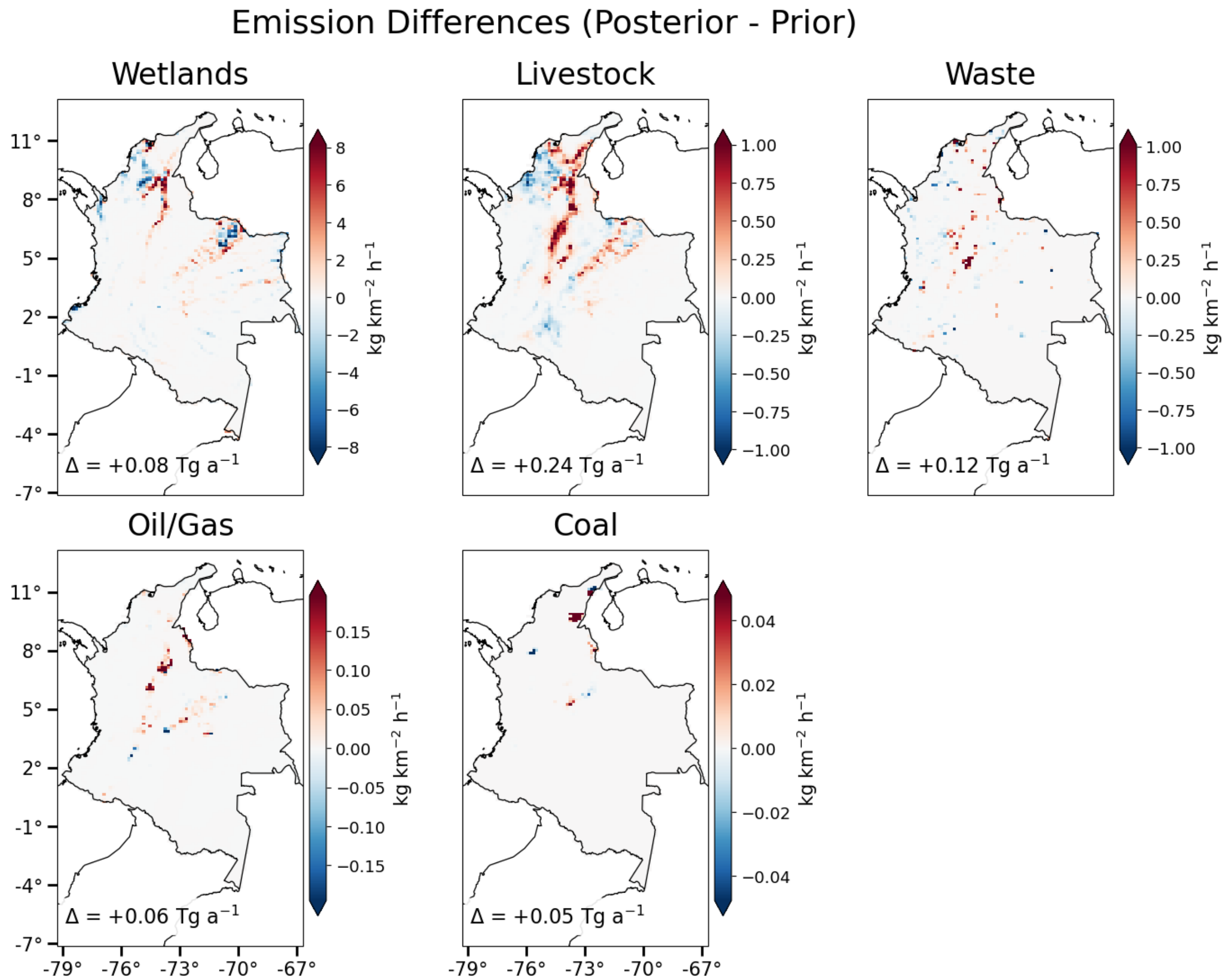


**Figure S5: Posterior minus prior methane emission differences for the major source sectors on the native inversion grid. Positive values indicate locations where the inversion increases emissions relative to the prior, while negative values indicate decreases. Panel annotations report the domain-total emission change for each sector in Tg a$^{-1}$.**

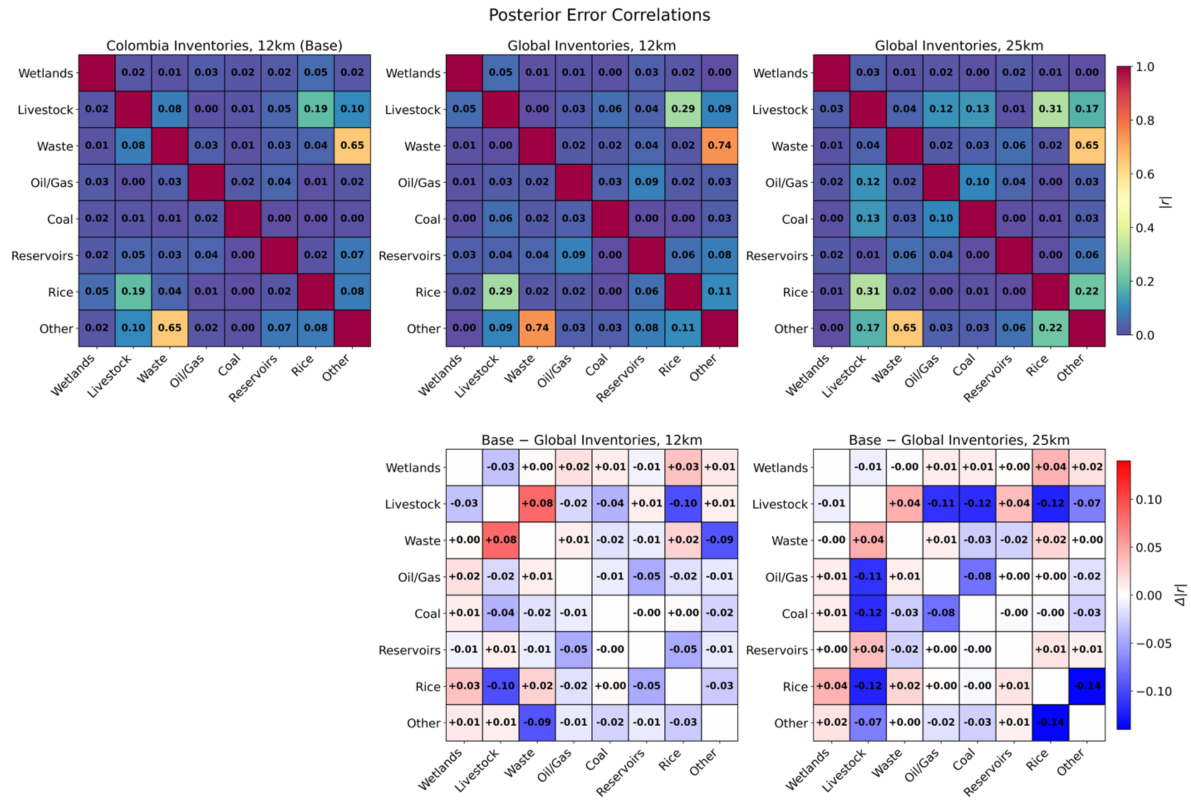


**Figure S6: Posterior error correlations between methane source sectors for different prior inventories and model resolutions. Top panels show the magnitude of posterior error correlations (|r|) for inversions using (left) Colombia-specific inventories at ~12 km × 12 km resolution (the base inversion), (middle) global inventories at ~12 km × 12 km, and (right) global inventories at ~25 km × 25 km. Bottom panels show the difference in error correlations (Δ|r|) between the base inversion and those using global inventories.**

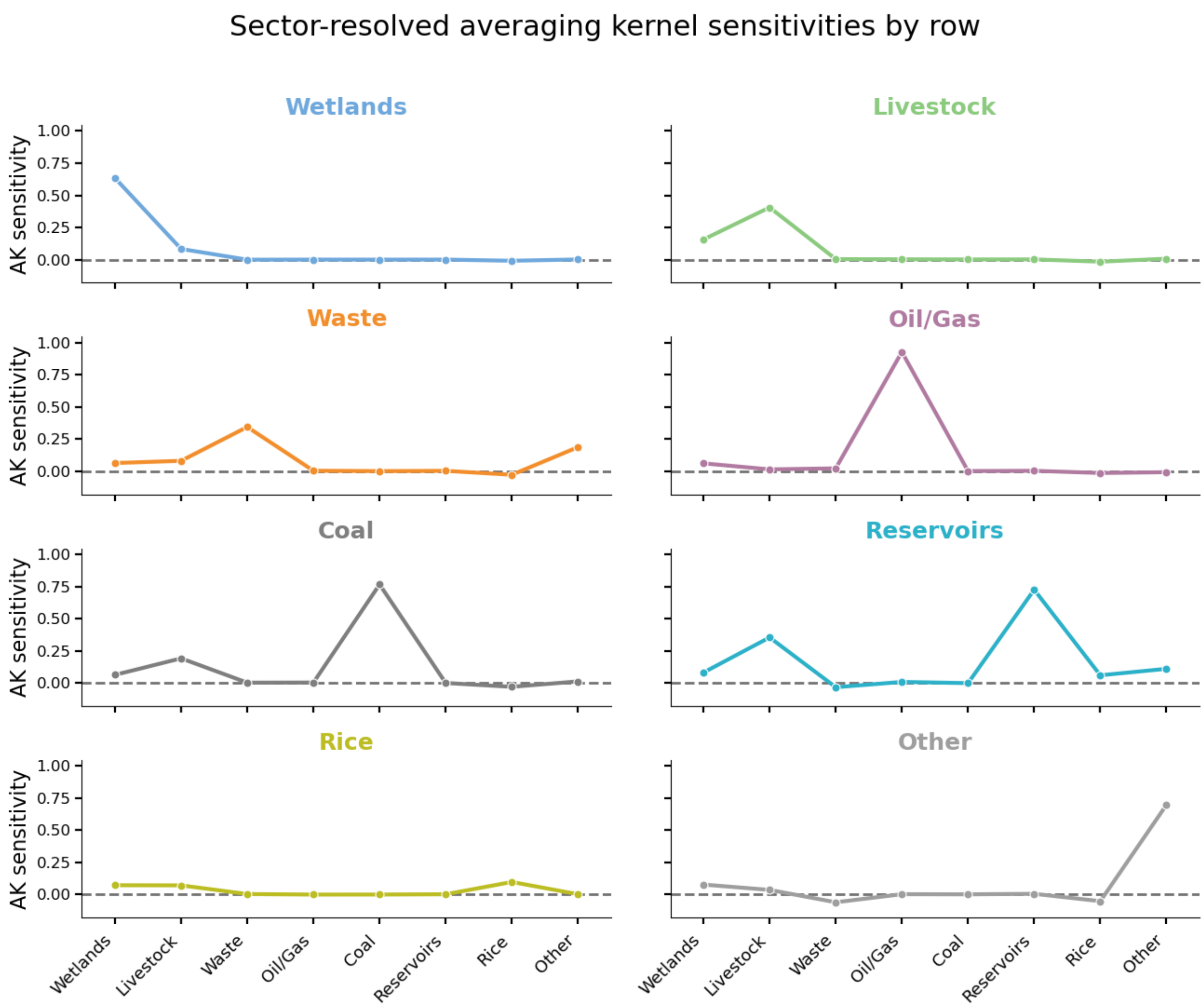


**Figure S7: Sector-resolved averaging kernel sensitivities for the aggregated methane source sectors, derived from the reduced averaging kernel matrix, $A_{\mathrm{red}}$. Each panel shows the sensitivity of the posterior estimate for the sector named in the panel title to perturbations in each aggregated source sector on the x-axis. Values on the sector's own x-axis position indicate how strongly that sector is constrained independently, whereas values at other x-axis positions indicate cross-sector coupling. The dashed horizontal line marks zero sensitivity.**

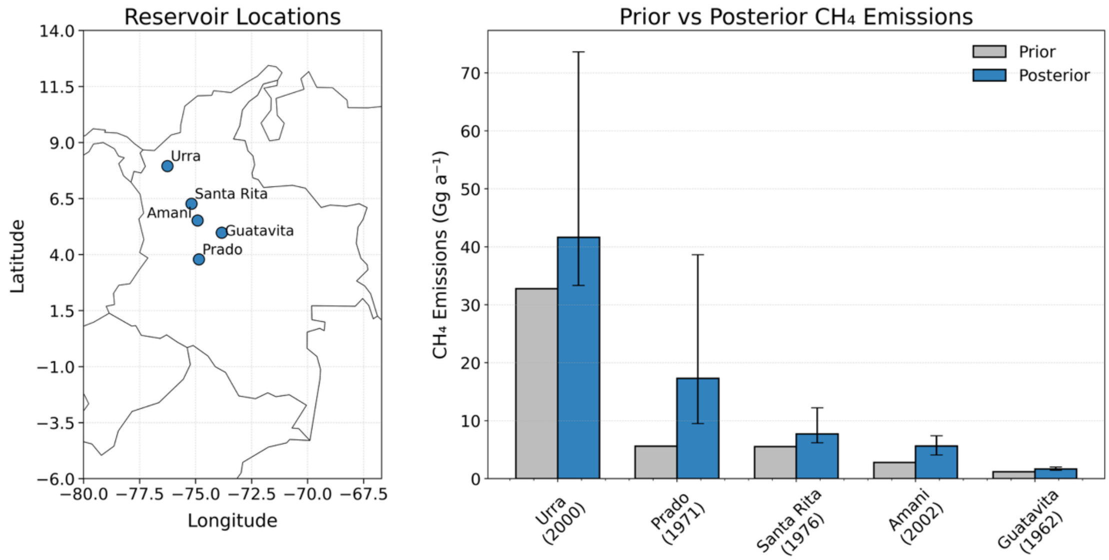


**Figure S8: Prior and posterior methane emissions for the six Colombian reservoirs that show emission adjustments across all inversion ensemble members. The map (left) shows the locations of the selected reservoirs, and the bar chart (right) compares prior and posterior emissions for each reservoir, with error bars indicating the range across the ensemble. Reservoir names and construction years from the GDW database are shown along the x-axis.**

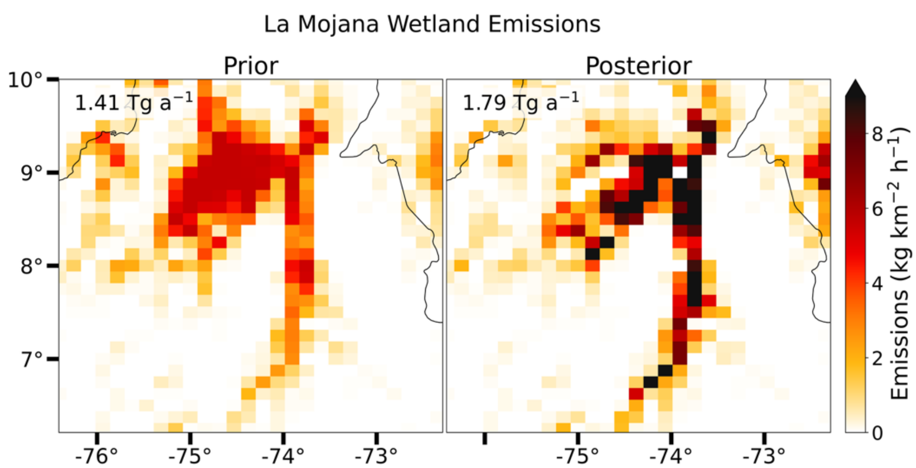


**Figure S9: Prior and posterior wetland emissions from GLWD+LPJ over La Mojana wetland region. The total wetland emissions over the region are given inset.**

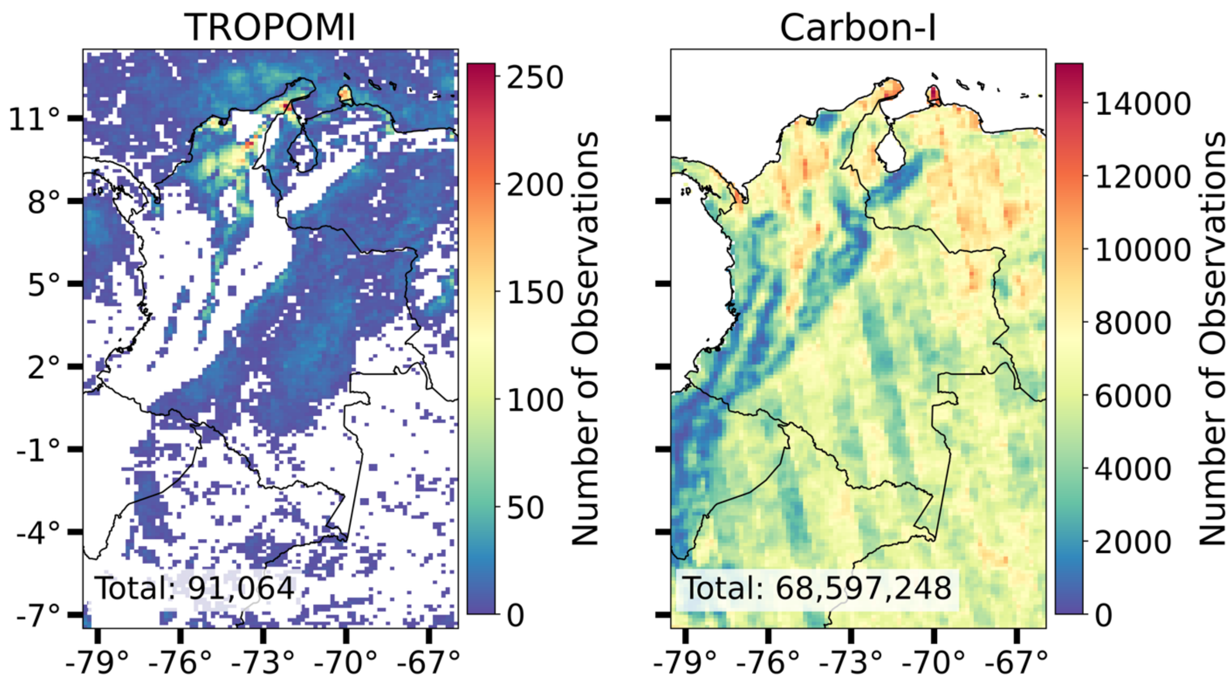


**Figure S10: Atmospheric methane observations from TROPOMI (left) and projected Carbon-I data (right) over Colombia. Carbon-I is one of the finalist missions in NASA's Earth System Explorers program, with a planned launch around 2030. It is designed to carry a SWIR imaging spectrometer capable of retrieving $CH_4$ at 400-m pixel resolution and is specifically optimized to achieve cloud-cleared observations over tropical wetlands (Carbon-I Team, 2024). Projected successful observation densities for Carbon-I were generated by combining simulated satellite orbits with high-resolution cloud cover data to estimate retrieval availability (Frankenberg et al., 2024). The figure shows the number of valid observations on the 0.125° × 0.15625° inversion grid for the year 2023. Grid cells with fewer than one valid observation are shown in white. TROPOMI provides 91,064 total observations over Colombia, while Carbon-I is projected to provide over 83 million observations. The increased observational density and coverage from Carbon-I would enable stronger constraints on emissions across Colombia.**